Croatian Society for Materials Protection

Metalurgija/Metallurgy

Vol. 65 No. 2 / 2026

Study on a Constitutive Model for Predicting Hot Deformation Behavior of 34CrNi3MoA Steel for Reducer of Mining Equipment

X. F. Zhang [1 2], C. F. Huang [3]*

https://doi.org/10.64486/m.65.2.5

[1] CCTEG Taiyuan Research Institute Co., Ltd., Shanxi, Taiyuan, China; mkyzxf@qq.com
[2] Shanxi Tiandi Coal Mining Machinery Co., Ltd., Shanxi, Taiyuan, China
[3] College of Mechanical Engineering, North China University of Science and Technology, Hebei, Tangshan, China
* Correspondence: 18831287238@163.com

Type of the Paper: Article
Received: August 13, 2025
Accepted: November 7, 2025

Abstract: As a high-strength medium-carbon quenched and tempered steel, 34CrNi3MoA is used in mining equipment reducer gears primarily due to its excellent mechanical properties, wear resistance, and impact resistance, meeting high-load demands under complex conditions. To develop an accurate constitutive model for predicting its high-temperature flow behavior, thermal compression tests were conducted on a Gleeble-3800 simulator at (1000–1200) °C and (0.01–10) s^{-1} strain rates. A strain-compensated Arrhenius model was established using test data, with its predictability analyzed via correlation coefficient (R) and average absolute relative error (ARRE). Results show the model accurately predicts flow behavior under these conditions, with R = 0.9933 and ARRE = 5.244 %. These findings provide a reference for initial design and numerical prediction of 34CrNi3MoA's high-temperature flow behavior, and are significant for numerical simulation and parameter optimization in its hot forming processes.

Keywords: 34CrNi3MoA steel; high-temperature flow behavior; constitutive model; reducer

1. Introduction

34CrNi3MoA is ideal for mining reducer gears due to its high strength, heat treatment adaptability, and wear resistance, enabling efficient power transmission under harsh conditions. Precise heat treatment and quality control are critical to fully utilize its potential. Finite element simulation has been applied to metal hot forming, where constitutive models predict material responses under loading, with their accuracy determining simulation reliability. Thus, a constitutive model for predicting 34CrNi3MoA's high temperature flow behavior is needed for performance analysis, simulation, and process optimization, to reveal its flow characteristics and advance engineering applications. Gao et al. [1-3] studied the fatigue crack growth behavior of 34CrNi3Mo high-strength steel and developed an innovative in-situ SEM method to determine the fatigue crack growth threshold via loading strategy adjustment. The study identified that crack tip orientation differences along various directions independent of slip system type control crack deflection. Zhang et al. [4,5] analyzed 34CrNi3MoV steel performance under various heat treatment parameters and optimized quenching/tempering

temperatures for better properties. Thus, studying 34CrNi3MoA thermal deformation, analyzing crankshaft bending/upsetting forging, and building dynamic recrystallization models are highly valuable for engineering [6-8]. The constitutive model is fundamental to describing stress-deformation relationships during thermal deformation, with accuracy critical for predicting material deformation laws. The Arrhenius model is widely used to characterize the effects of temperature and strain rate on true stress in high-temperature metal deformation. Zou et al. [9-11] employed the phenomenological Arrhenius equation to calculate the activation energy of 34CrNi3MoV steel under varying strain parameters, constructing a kinetic model for predicting dynamic recrystallization volume fraction via numerical fitting. Zhu et al. [12-15] integrated the theoretical Arrhenius model with finite element analysis to study processing parameter effects on Ti65 alloy mechanical behavior during multi-directional forging MDF, determining an optimal initial temperature of 1000 °C and showing that increasing forging speed raises temperature and maximum principal stress.

This paper studies the high – temperature deformation constitutive model of forged 34CrNi3MoA steel. Considering the effects of strain rate, temperature, and strain, a strain – compensated Arrhenius constitutive model for 34CrNi3MoA steel is established. The accuracy of the model is evaluated based on the linear correlation coefficient and the absolute value of the average relative error, aiming to provide theoretical guidance for the thermal deformation process of 34CrNi3MoA steel.

2. Materials and Methods

2.1. Hot compression test procedure

The experimental material used in this study is 34CrNi3MoA steel, and its main chemical composition is listed in Table 1. Cylindrical specimens with dimensions of Φ8 mm × 12 mm were machined by wire cutting. Single-pass hot compression tests were performed on a Gleeble-3800 thermal simulator. The test temperatures were set to 1000 °C, 1100 °C, and 1200 °C, with strain rates of 0.01 s^{-1}, 0.1 s^{-1}, 1 s^{-1}, and 10 s^{-1}, and a total compression deformation of 60 %. During testing, the specimens were heated to the target temperature at a rate of 100 °C/min, held for 3 minutes, and then compressed under the preset temperature and strain rate conditions [16,17].

Table 1. Chemical composition of 34CrNi3MoA steel / wt. %

C	Si	Mn	S	P	Cr	Ni	Mo	Cu
0.30–0.40	0.30–0.50	0.60–0.90	≤ 0.025	≤ 0.025	0.70–1.10	2.75–3.25	0.25–0.40	≤ 0.25

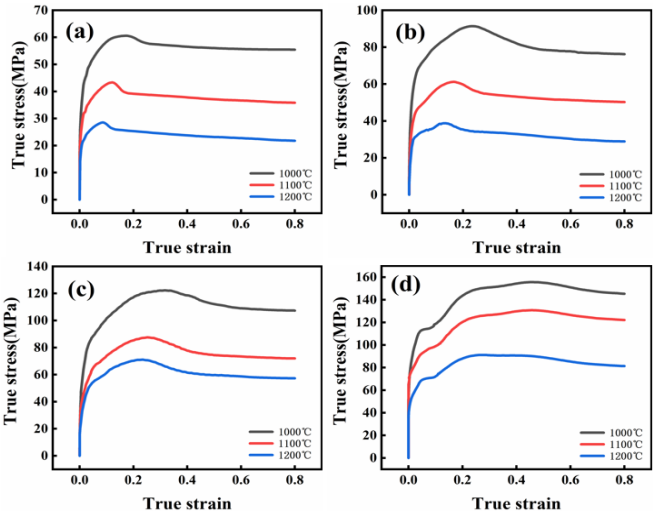

Figure 1. The true stress-strain curves of 34CrNi3MoA steel under different strain rates.

（a）0.01 s^{-1}；（b）0.1 s^{-1}；（c）1 s^{-1}；（d）10 s^{-1}

https://doi.org/10.64486/m.65.2.5

Figure 1 shows the true stress-true strain curves of 34CrNi3MoA steel under different deformation conditions. Analysis indicates temperature strongly affects flow stress: strain hardening occurs across the strain range, with hardening intensity decreasing as strain increases, suggesting work hardening dominates. However, rising temperature induces softening that overrides hardening and controls stress flow, evident as flow stress declining or stabilizing after peaking with increasing strain. The material also displays significant strain rate sensitivity under tested conditions, with sensitivity varying notably across temperatures.

2.2. Constitutive model

Plastic deformation in metals involves complex interactions of multiple factors. Existing research shows that the relationship between flow stress and deformation parameters during metal plastic deformation can be described by the Arrhenius model, expressed as [18-20].

$$\dot{\varepsilon} = Af(\sigma)\exp(\frac{-Q}{RT}) \tag{1}$$

$$f(\sigma) = \begin{cases} \sigma^m, \alpha\sigma < 0.8 \\ \exp(\beta\sigma), \quad \alpha\sigma > 1.2 \\ [\sinh(\alpha\sigma)]^n, \quad \text{for all } \sigma \end{cases} \tag{2}$$

In the equation, $\dot{\varepsilon}$ is the strain rate, T is the deformation temperature, Q *is the t*hermal deformation activation energy J/mol, R is the molar gas constant (8.314 J / mol · K), A, β, α, m and n are material constants.
At a constant deformation temperature, equations (1) and (2) were combined and differentiated to obtain:

$$\begin{cases} m = \left[\dfrac{\partial \ln \dot{\varepsilon}}{\partial \ln \sigma}\right]_T \\ \beta = \left[\dfrac{\partial \ln \dot{\varepsilon}}{\partial \sigma}\right]_T \\ n = \left[\dfrac{\partial \ln \dot{\varepsilon}}{\partial \ln(\sinh(\alpha\sigma))}\right]_T \end{cases} \tag{3}$$

Extract peak stress data corresponding to different deformation parameters from the stress-strain curve shown in Figure 1. Using Origin software, linear fitting was performed on $ln\dot{\varepsilon}-\dot{l}n\sigma_p$ and $ln\dot{\varepsilon} - \sigma_p$ separately, and the fitting results are shown in Figure 2(a) and Figure 2(b). As shown in the figure, the slopes of the fitted lines are roughly similar. After calculation, taking the average of these slopes, m is obtained as 6.34. Using this method, by analyzing the fitted data in Figure 2(b), β was found to be 0.086, and then α was calculated to be 0.0132 based on $\alpha=\beta / m$. Similarly, when the strain rate F remains constant, draw a fitted line for $ln\dot{\varepsilon} - ln[\sinh(\alpha\sigma_p)]$, and the result is shown in Figure 2(c). Calculate the mean slope of the fitted line under different deformation conditions, with n = 4.66. Plot and fit with $1/T$ as the x-axis and $\ln[\sinh(\alpha\sigma_p)]$ as y-axis, and take the average slope of the fitted line to obtain Q_{act} / Rn_1 = 8446.36. Substitute the values of R and n obtained above into Q_{act} / Rn_1 = 8446.36 and finally calculate the deformation activation energy Q_{act} = 327157.63 J/mol.

https://doi.org/10.64486/m.65.2.5

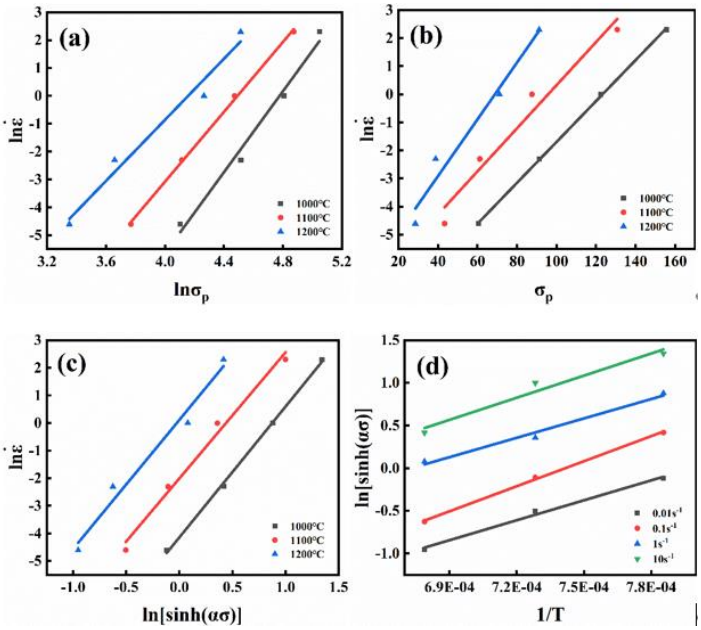

Figure 2. Fitting diagram（a）$ln\dot{\varepsilon}-ln\sigma$； （b）$ln\dot{\varepsilon}-\sigma$； （c）$ln\dot{\varepsilon}-ln[sinh(\alpha\sigma)]$； （d）$\ln[\sinh(\alpha\sigma_p)]-1/T$

The Zener Hollomon parameter, commonly referred to as the Z-parameter, is mainly used to characterize the intrinsic relationship between the deformation temperature, strain rate, and flow stress of materials. Its expression is as follows [21].

$$Z = \dot{\varepsilon}\exp(Q/RT) \tag{4}$$

By combining equation (2) with the above equation and modifying it, we can obtain:

$$\ln Z = \ln A + n\ln[\sinh(\alpha\sigma)] \tag{5}$$

For different deformation conditions, scatter plots of ln$Z$ versus $\ln[\sinh(\alpha\sigma_p)]$ were plotted and subjected to linear fitting. Analysis indicates that the intercept of the fitted line corresponds to the value of ln$A$, and calculation yields $A = 6.2794\times10^{11}$.

Systematically organize and summarize all parameters involved in the previous research process, and substitute them into equations. After this step, the Arrhenius peak stress constitutive model suitable for 34CrNi3MoA steel was successfully constructed as follows:

$$\dot{\varepsilon} = 6.2794\times10^{11}\left[0.0132\sinh\left(\sigma_p\right)\right]^{4.66}\exp\left(-\frac{327157.63}{8.314T}\right) \tag{6}$$

3. Results

3.1. Strain compensation Arrhenius constitutive model

To validate the Arrhenius model's accuracy, a strain compensation mechanism for flow stress was introduced to develop a more precise strain-coupled constitutive model. Following the above procedure, material constants Q, n, a, and ln$A$ in the Arrhenius equation were solved and calculated. After obtaining these values, fitting was performed, with results shown in Figure 3.

https://doi.org/10.64486/m.65.2.5

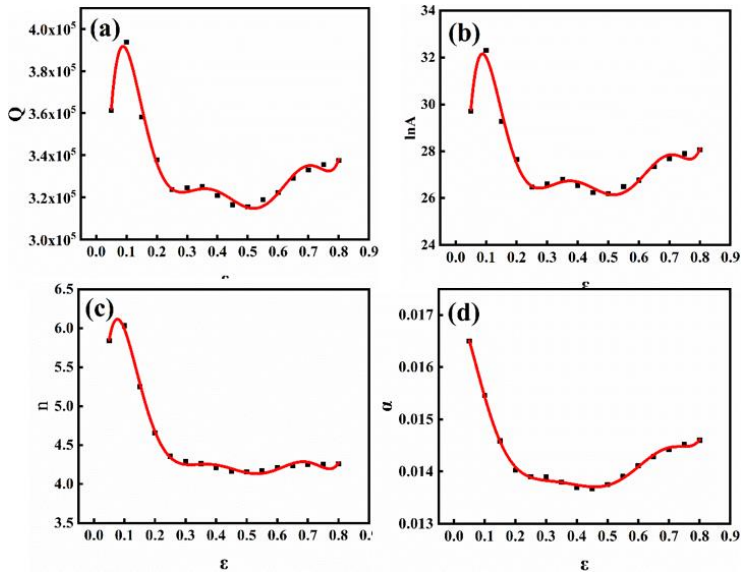

Figure 3. Fitting diagram（a）$Q-\varepsilon$ ；（b）$\ln A-\varepsilon$ ；（c）$n-\varepsilon$ ；（d）$\alpha-\varepsilon$

The relationship between the material constants and strain was fitted using a polynomial (equation 7).

$$G=k_0+k_1\varepsilon+k_2\varepsilon^2+k_3\varepsilon^3+k_4\varepsilon^4+k_5\varepsilon^5+\cdots\cdots \tag{7}$$

After evaluating polynomial orders from 1~9 via iterative calculations, a sixth-order polynomial was selected as optimal. Coefficients are listed in Table 2.

Table 2. Fitting equation for material related constants of 34CrNi3MoA steel

Coefficient	*n*	α	*LnA*	Q
k_0	2.861	0.017	12.390	150768
k_1	110.304	0.0017	614.872	7.45E+06
k_2	-1300.220	-0.395	-6871.89	-8.29E+07
k_3	6636.005	2.927	35047.28	4.22E+08
k_4	-17851.228	-9.581	-95176.9	-1.15E+09
k_5	26397.500	16.183	142193.1	1.72E+09
k_6	-20288.844	-13.713	-110203	-1.34E+09
k_7	6333.352	4.610	34606.12	4.21E+08

The constitutive equation of 34CrNi3MoA steel under the introduction of strain factor is:

$$\sigma=\frac{1}{\alpha}\ln\left\{\left(\frac{Z}{A}\right)^{\frac{1}{n}}+\left[\left(\frac{Z}{A}\right)^{\frac{2}{n}}+1\right]^{\frac{1}{2}}\right\} \tag{8}$$

3.2. Verification Model

To test the predictive ability of the Arrhenius constitutive model for strain compensation mechanism, the flow stress data obtained from actual hot compression experiments were compared and analyzed with the flow

https://doi.org/10.64486/m.65.2.5

stress values predicted by the constitutive equation. Based on the above data, a comparison chart was drawn, as shown in Figure 4.

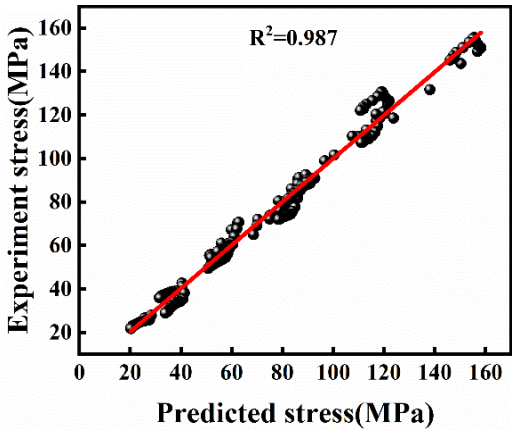

Figure 4. Comparison between predicted values and experimental values

From Figure 4, it can be seen that the experimental data is highly consistent with the predicted values of the constitutive model, which fully indicates that the strain compensated Arrhenius constitutive equation has a high model prediction accuracy. To more accurately analyze the accuracy of the equation's prediction results, standard statistical parameters are used to analyze and calculate the correlation coefficient R and the average absolute error AARE (%). The specific calculation equation is as follows:

$$R = \frac{\sum_{i=1}^{N}\left(\sigma_{Ei} - \overline{\sigma_E}\right)\left(\sigma_{P_i} - \overline{\sigma_{P_i}}\right)}{\sqrt{\sum_{i=1}^{N}\left(\sigma_{Ei} - \overline{\sigma_E}\right)^2 \sum_{i=1}^{N}\left(\sigma_{Pi} - \overline{\sigma_{Pi}}\right)^2}} \tag{9}$$

$$AARE(\%) = \frac{1}{N}\sum_{i=1}^{N}\left|\frac{\sigma_{Ei} - \sigma_{Pi}}{\sigma_{Ei}}\right| \tag{10}$$

In the equation: N - total number of data; σ_{Ei}、$\overline{\sigma_E}$ - experimental values and the average of experimental values, MPa; σ_{Pi}、$\overline{\sigma_{Pi}}$ - the predicted value and the average of the predicted values, MPa。

A larger correlation coefficient R indicates stronger correlation, while a smaller average absolute relative error AARE percentage signifies closer agreement between predicted and experimental values. Calculations show R is 0.9933 and AARE is 5.244 percent, demonstrating that the 34CrNi3MoA steel constitutive model developed herein exhibits high accuracy and provides reliable basic data for subsequent crankshaft forming numerical simulations.

To check whether the grain size of the forging material has been refined, metallographic experiments were conducted on the material sample. Figure 5 shows a schematic diagram of the microstructure of the material sample.

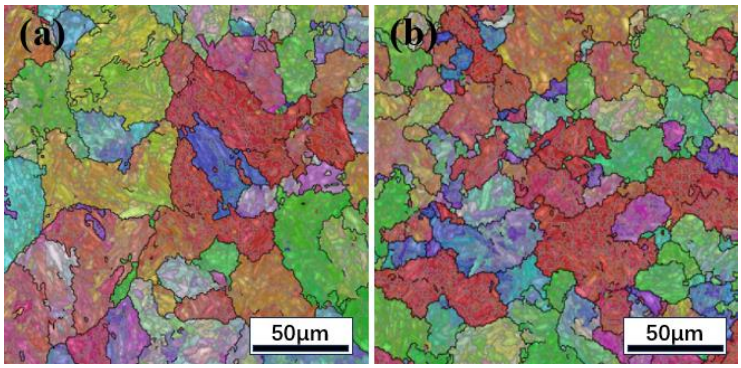

Figure 5. Microstructure analysis of 34CrNi3MoA material at different positions

https://doi.org/10.64486/m.65.2.5

4. Discussion

This study focuses on 34CrNi3MoA steel used for mining equipment reducers, based on isothermal compression experiments. A systematic investigation of its hot deformation and dynamic recrystallization behavior was conducted to establish a theoretical and experimental foundation for the forging process of 34CrNi3MoA and to support its application in high-strength components such as crankshafts and gun barrels.

The stress–strain curves of 34CrNi3MoA steel under different deformation conditions were successfully obtained through isothermal compression tests. Based on the experimental data, a strain-compensated Arrhenius constitutive equation was developed. This model can predict and analyze the stress evolution of metal materials during the bending and upsetting stages of crankshaft and crankcase forming. The model's predictive performance was evaluated using the correlation coefficient (R) and the average absolute relative error (AARE), confirming that the established model provides high accuracy and reliable predictive capability.

Microstructure analysis was also performed to examine the material at different positions after deformation.

5. Conclusion

The flow stress of 34CrNi3MoA steel increases with decreasing temperature and increasing strain rate. Based on experimental data and the Arrhenius constitutive relationship, a strain-compensated constitutive equation for forged 34CrNi3MoA steel was established. The correlation coefficient (R = 0.9933) and the average absolute relative error (AARE = 5.244 %) demonstrate that the developed model achieves high predictive accuracy and can provide theoretical guidance for the development and optimization of the hot forming process of this steel.

Acknowledgments: This work is supported by the Key project of Tiandi Science and Technology (2024-TD-ZD003-02).

References

[1] Y. Hu, D. Zhang, L. Xu, *et al*., "Effect of Notch on Fatigue Performance of Marine Shaft Made of 34CrNi3Mo Alloy Steel Under Torsional Loading," *International Journal of Fatigue*, vol. 175, p. 107790, 2023. https://doi.org/10.1016/j.ijfatigue.2023.107790

[2]X. Q. Lang and Y. S. Fang, "Factors Affecting the Impact of 34CrNi3MoA Material," *Valve*, (in Chinese) no. 02, pp. 228–231, 2024.

[3] Y. Gao, G. Sui, H. Li, *et al*., "In-Situ Investigation of Fatigue Crack Growth Behavior of 34CrNi3Mo High-Strength Steel," *Materials Letters*, vol. 358, p. 135793, 2024. https://doi.org/10.1016/j.matlet.2023.135793

[4] H. Q. Zhang, Z. Y. Xie, X. Zhu, *et al*., "Optimization of Heat Treatment Process for 34CrNi3MoV Steel Box," *Metal Heat Treatment*, vol. 48, no. 05, pp. 224–228, 2023. (in Chinese) Available: https://qikan.cmes.org/jsrcl/EN/10.13251/j.issn.0254-6051.2023.05.034

[5] Z. P. Zou, D. Xu, Y. C. Ren, *et al*., "Dynamic Recrystallization Behavior of 34CrNi3MoV Alloy Steel," *Metal Heat Treatment*, vol. 48, no. 05, pp. 32–40, 2023. (in Chinese) Available: https://qikan.cmes.org/jsrcl/EN/10.13251/j.issn.0254-6051.2023.05.006

[6] P. Zhu, S. Yang, Z. Gao, *et al*., "Optimization of Hot Deformation Parameters for Multi-Directional Forging of Ti65 Alloy Based on the Integration of Processing Maps and Finite Element Method," *Journal of Materials Research and Technology*, vol. 29, pp. 5271–5281, 2024. https://doi.org/10.1016/j.jmrt.2024.06.099

[7] Y. Liu, M. Li, X.-W. Ren, *et al*., "Flow Stress Prediction of Hastelloy C-276 Alloy Using Modified Zerilli–Armstrong, Johnson–Cook and Arrhenius-Type Constitutive Models," *Transactions of Nonferrous Metals Society of China*, vol. 30, no. 11, pp. 3031–3042, 2020. https://doi.org/10.1016/S1003-6326(20)65350-9

https://doi.org/10.64486/m.65.2.5

[8] I.-K. Jin, J.-G. Lee, Y.-J. Lee, *et al*., "Microstructure Control and Dynamic Recrystallization Behavior Analysis in Hot Forging of Metastable Beta Ti-5Mo-4Fe Alloy," *Journal of Alloys and Compounds*, vol. 1010, p. 178125, 2025. https://doi.org/10.1016/j.jallcom.2024.178125

[9] C. Liu, S. Barella, Y. Peng, *et al*., "Modeling and Characterization of Dynamic Recrystallization Under Variable Deformation States," *International Journal of Mechanical Sciences*, vol. 238, p. 107838, 2023. https://doi.org/10.1016/j.ijmecsci.2022.107838

[10] R. Ranjan and A. Meena, "Dynamic Recrystallization Characteristics and Processing Map Development of Mn-Ni-Mo Steel Using Constitutive Modeling," *Materials Science and Engineering: A*, vol. 923, p. 147672, 2025. https://doi.org/10.1016/j.msea.2024.147672

[11] X. Huang, Y. Zang, H. Ji, *et al*., "Combination Gear Hot Forging Process and Microstructure Optimization," *Journal of Materials Research and Technology*, vol. 19, pp. 1242–1259, 2022. https://doi.org/10.1016/j.jmrt.2022.05.089

[12] M. K. Razali, Y. Heo, M. Irani, *et al*., "Grain Size Prediction in SCR420HB Hot Forging: Combining Phenomenological and JMAK Models With Experimental and Numerical Analysis," *Materials Today Communications*, vol. 41, p. 110921, 2024. https://doi.org/10.1016/j.mtcomm.2024.110921

[13] S. Zhu, J. Cong, W. Yuan, *et al*., "Simulation of Heavy-Duty Crankshaft Sub-Dynamics and Experimental Study of Wear Mechanisms," *Materials Today Communications*, vol. 36, p. 106826, 2023. https://doi.org/10.1016/j.mtcomm.2023.106826

[14] X. Wu-Jiao, W. Kai-Qing, Z. Jie, *et al*., "Experimental and Computational Failure Analysis of TR Upset-Bending Equipment for Heavy Crankshaft With Continuous Grain Flow," *Engineering Failure Analysis*, vol. 17, no. 2, pp. 546–554, 2010. https://doi.org/10.1016/j.engfailanal.2009.09.010

[15] Z. Hu, J. Zheng, L. Hua, *et al*., "Investigation of Forging Formability, Microstructures and Mechanical Properties of Pre-Hardening Al-Zn-Mg-Cu Alloy," *Journal of Manufacturing Processes*, vol. 131, pp. 2082–2100, 2024. https://doi.org/10.1016/j.jmapro.2024.06.064

[16] F. Li, C. Zhu, S. Li, *et al*., "A Comparative Study on Modified and Optimized Zerilli–Armstrong and Arrhenius-Type Constitutive Models to Predict the Hot Deformation Behavior in 30Si2MnCrMoVE Steel," *Journal of Materials Research and Technology*, vol. 20, pp. 3918–3929, 2022. https://doi.org/10.1016/j.jmrt.2022.07.127

[17] Y. Fu, M. Zhang, X. Chen, *et al*., "Hot Deformation Behavior and Process Optimization of TC4-DT Alloy Fabricated by Wire and Arc Additive Manufacturing With In-Situ Forging," *Journal of Materials Research and Technology*, vol. 30, pp. 5056–5068, 2024. https://doi.org/10.1016/j.jmrt.2024.02.024

[18] P. Luo, C. Hu, Q. Wang, *et al*., "Microstructure Simulation and Experimental Investigation of Dynamic Recrystallization for Ultra-High-Strength Steel During Hot Forging," *Journal of Materials Research and Technology*, vol. 26, pp. 4310–4328, 2023. https://doi.org/10.1016/j.jmrt.2023.07.079

[19] R. Hino, A. Sasaki, F. Yoshida, *et al*., "A New Algorithm for Reduction of Number of Press-Forming Stages in Forging Processes Using Numerical Optimization and FE Simulation," *International Journal of Mechanical Sciences*, vol. 50, no. 5, pp. 974–983, 2008. https://doi.org/10.1016/j.ijmecsci.2007.09.009

[20] Y. Kim, H. Y. Jeong, J. Park, *et al*., "Optimizing Process Parameters for Hot Forging of Ti-6242 Alloy: A Machine Learning and FEM Simulation Approach," *Journal of Materials Research and Technology*, vol. 27, pp. 8228–8243, 2023. https://doi.org/10.1016/j.jmrt.2023.06.062

https://doi.org/10.64486/m.65.2.5

[21] L. Zhang, W. Yang, Q. Cheng, *et al*., "The Effect of Different Forging Ratios on the Properties and Microstructures of High-Strength Steel 40CrNi2Si2MoV," *Journal of Materials Research and Technology*, vol. 29, pp. 2326–2338, 2024. https://doi.org/10.1016/j.jmrt.2024.04.062

https://doi.org/10.64486/m.65.2.5